ATMO 611 – Satellite Data Applications

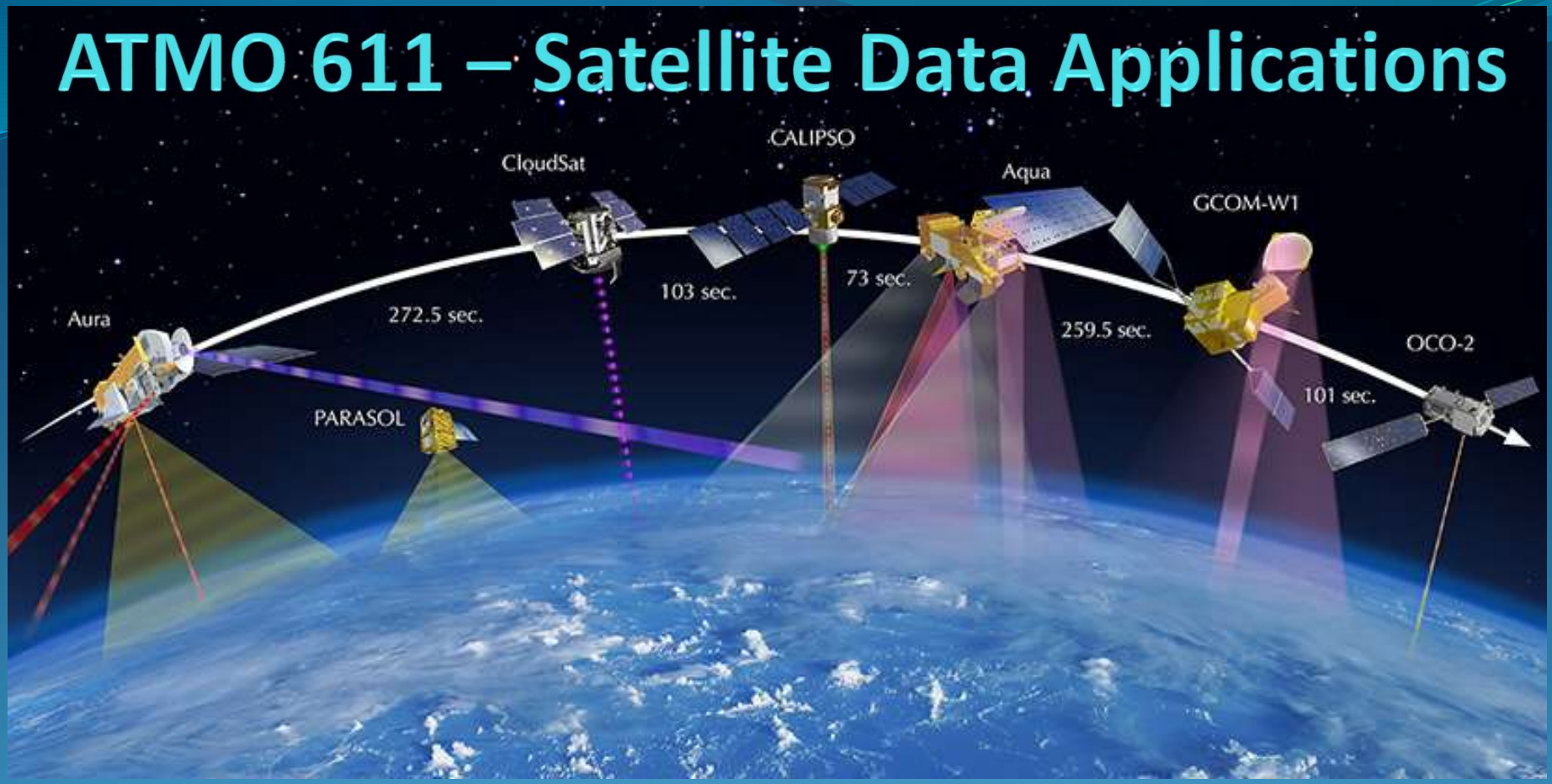

Course Introduction
Lecture 2: Satellite Overview

Jennifer D. S. Griswold

Lab Topics & Satellites Data Covered

- **A-Train**
  - **Polar Orbiting**
  - **MODIS**
  - **OMI**
  - **CloudSat/CALIPSO**
- **Other Data**
  - **TRMM**
  - **GPCP**
  - **TOMS**
- **Types of Data**
  - **Clouds**
  - **Aerosol**
  - **Land Products**
  - **Ocean Products**
  - **Precipitation**
- **Reanalysis Data**
  - **Meteorology**

Introduction to Remote Sensing
Survey of Satellites we will be covering
Lab 0: Project Description Review
Term Project Outline – Previous Projects - Brainstorming
Introduction to MODIS Instrumentation
Lab 1: Introduction to MODIS, Matlab and File Types
MODIS Products (L2 vs. L3) and Data Access
Introduction to MODIS Cloud Products
LAB 2: Global and Regional Cloud Properties
Introduction to CloudSat/CALIPSO Cloud Products and Data
CALIPSO "Curtains" and Analysis
LAB 3: Case Studies using CALIPSO "Curtains"
Introduction to MODIS Aerosol Products
MODIS Aerosol Products Continued
LAB 4: Regional MODIS Aerosol Changes & Trends
Introduction to TOMS and OMI Satellites
Introduction to Absorbing Aerosol Index and Aerosol Index
LAB 5: Comparison of AAI, AI, Optical Depth and Thickness
Introduction to CALIOP Aerosol
CALIOP Aerosol identification
LAB 6: Cloud Aerosol Interactions - CALIPSO and CALIOP
Introduction to Land Surface Products
MODIS Fire, Burned Area and other Useful Datasets
LAB 7: Mapping Land Use Changes and Fires
Intro to Ocean Products: Temperature & Topography
Mapping El Niño
LAB 8: Mapping Major El Niño Events
Introduction to TRMM Satellite
TRMM Data Products
LAB 9: Precipitation Trends and Patterns
Introduction to GPCP Data Set
Daily, Monthly, and Climatological Precipitation
LAB 10: Comparison between TRMM and GPCP Data Sets

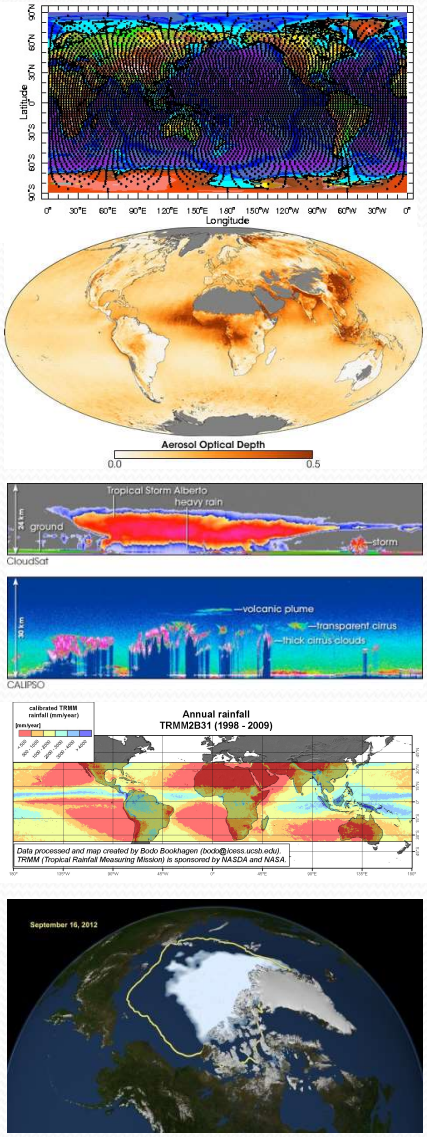

MODIS Satellite Overview

- **Different MODIS teams produce the various products that we use, each with their own websites**
  - **ATMOSPHERE** – Cloud and Aerosol Properties
  - **LAND** – Albedo, Surface Reflectance, Burned Area Index
  - **OCEAN** – Ocean Color, SST, Chlorophyll

MODIS Atmosphere Time Resolution

- **Data is available at different time resolutions.**
- **Level 2 data (L2) are called Granules and represent 5 minutes of data (also high spatial resolution).**
- **Level 3 (L3) are available in three different time resolutions (lower spatial resolution, 1 x 1 degree)**
  - Daily (08_D3)
  - Eight Day (08_E3)
  - Monthly (08_M3)
- **It is necessary to choose the time resolution (and spatial resolution) that suits your research needs.**

Atmosphere Products

- https://modis-atmos.gsfc.nasa.gov/products

- **There are six Level-2 (Orbital Swath/Granule) MODIS Atmosphere products collected from two platforms: the Terra platform and the Aqua platform.**
  - **Aerosol** - MOD04_L2 (Terra) and MYD04_L2 (Aqua)
  - **Cloud** - MOD06_L2 (Terra) and MYD06_L2 (Aqua)
  - **Water Vapor** - MOD05_L2 (Terra) and MYD05_L2 (Aqua)
  - **Atmospheric Profile** - MOD07_L2 (Terra) and MYD06_L2 (Aqua)
  - **Cloud Mask** - MOD35_L2 (Terra) and MYD35_L2 (Aqua)
  - **Joint Atmosphere** - MODATML2 (Terra) and MYDATML2 (Aqua)

MODIS Aerosol 04_L2

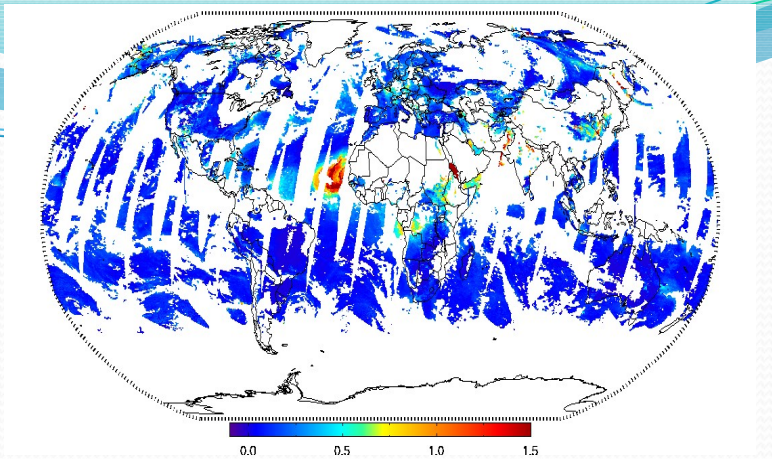

- **Global Aerosol**
  - ambient aerosol optical thickness and depth (AOT; AOD)
  - non-cloudy conditions during the day, not over ice and snow
  - Primary Products 10 x 10 km.
  - AOT is derived over ocean and dark vegetated surfaces at 3 km resolution, and contained in MOD04_3K and MYD04_3K product files for Terra and Aqua.
  - There are two 'flavors' of Aerosol retrieval algorithms:
    - Dark Target and Deep Blue

MODIS Aerosol Research Examples

Global Estimates of Ambient Fine Particulate Matter Concentrations from Satellite-Based Aerosol Optical Depth: Development and Application

Aaron van Donkelaar,[1] Randall V. Martin,[1,2] Michael Brauer,[3] Ralph Kahn,[4] Rob and Paul J. Villeneuve[5,6]

[1]Department of Physics and Atmospheric Science, Dalhousie University, Halifax, Nova Scotia, for Astrophysics, Cambridge, Massachusetts, USA; [3]School of Environmental Health, Universi Canada; [4]N Toronto, O

AGU PUBLICATIONS

Earth and Space Science

RESEARCH ARTICLE
10.1002/2017EA000288

Key Points:
- Historical CMIP5 model runs that include cloud-aerosol interactions underestimate AOD by 15% and CF by 10% overall on a global scale
- A regional analysis biomass burning regions (South America and South Africa) show agreement in timing of AOD and CF minima and maxima
- Monthly model and satellite data are insufficient to replicate observed relationships between CF and AOD seen in daily data

Correspondence to:
J.D Small Griswold,
smallgri@hawaii.edu

Citation:
Sockol A, and J. D. Small Griswold (2017), Intercomparison between CMIP5 model and MODIS satellite-retrieved data of aerosol optical depth, cloud fraction, and cloud-aerosol interactions, *Earth and Space Science*, 4, doi:10.1002/2017EA000288.

Intercomparison between CMIP5 model and MODIS satellite-retrieved data of aerosol optical depth, cloud fraction, and cloud-aerosol interactions

Alyssa Sockol[1] and Jennifer D. Small Griswold[1]

[1]Atmospheric Sciences Department, University of Hawai'i at Mānoa, Honolulu, Hawaii, USA

Abstract Aerosols are a critical component of the Earth's atmosphere and can affect the climate of the Earth through their interactions with solar radiation and clouds. Cloud fraction (CF) and aerosol optical depth (AOD) at 550 nm from the Moderate Resolution Imaging Spectroradiometer (MODIS) are used with analogous cloud and aerosol properties from Historical Phase 5 of the Coupled Model Intercomparison Project (CMIP5) model runs that explicitly include anthropogenic aerosols and parameterized cloud-aerosol interactions. The models underestimate AOD by approximately 15% and underestimate CF by approximately 10% overall on a global scale. A regional analysis is then used to evaluate model performance in two regions with known biomass burning activity and absorbing aerosol (South America (SAM) and South Africa (SAF)). In SAM, the models overestimate AOD by 4.8% and underestimate CF by 14%. In SAF, the models underestimate AOD by 35% and overestimate CF by 13.4%. Average annual cycles show that the monthly timing of AOD peaks closely match satellite data in both SAM and SAF for all except the Community Atmosphere Model 5 and Geophysical Fluid Dynamics Laboratory (GFDL) models. Monthly timing of CF peaks closely match for all models (except GFDL) for SAM and SAF. Sorting monthly averaged 2° × 2.5° model or MODIS CF as a function of AOD does not result in the previously observed "boomerang"-shaped CF versus AOD relationship characteristic of regions with absorbing aerosols from biomass burning. Cloud-aerosol interactions, as observed using daily (or higher) temporal resolution data, are not reproducible at the spatial or temporal resolution provided by the CMIP5 models.

Annual cycle of global distributions of aerosol optical depth from integration of MODIS retrievals and GOCART model simulations

Hongbin Yu, R. E. Dickinson, and M. Chin[1]

ogy, Atlanta, Georgia, USA

nbelt, Maryland, USA

nbelt, Maryland, USA

ber 2002; published 14 February 2003.

neter (MODIS) instrument onboard
s an unprecedented opportunity to
n a nearly global scale. However,
d lands introduces significant gaps in
e other means. This study provides a
sol optical depth by combining the
Ozone Chemistry Aerosol Radiation
the uncertainties in each product.
better correlated with the ground-
irements than are either the MODIS
ps in the MODIS retrievals are filled
ERONET aerosol climatology. The
ment with the Advanced Very High
y over the Atlantic and North Indian
MODIS retrievals in 2001 and the
y a result of extremely active
North America in the year 2001.
ic and South Indian Oceans may be
e model and/or cloud, whitecap, and
TERMS: 0305 Atmospheric Composition and
ic Composition and Structure: Pollution—
Structure: Troposphere—composition and
logy and Atmospheric Dynamics: Numerical

MODIS Cloud 06_L2

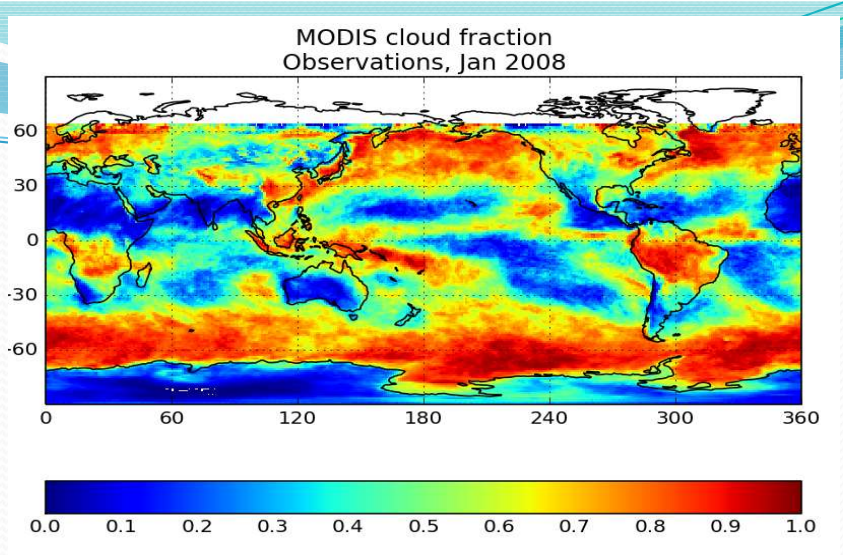

- **Global Cloud**
  - Monitors the physical and radiative properties of clouds
    - cloud fraction
    - effective cloud particle radius
    - cloud optical thickness
    - cloud shadow effects
    - cloud top temperature and height
    - effective emissivity
    - cloud phase (ice vs. water, opaque vs. non-opaque)
    - cloud particle phase (ice vs. water, clouds vs. snow)
  - both daytime and nighttime conditions

MODIS Cloud Research Examples

Reconciling Simulated and Observed Views of Clouds: MODIS, ISCCP, and the Limits of Instrument Simulators

ROBERT PINCU
University of Colorado, and NOAA/Earth System Research Laborat
STEVEN PLATNI
Earth Sciences Division, NASA Goddard Space Fl

Aerosol invigoration and restructuring of Atlantic convective clouds

Ilan Koren,[1,2] Yoram J. Kaufman,[1] Daniel Rosenfeld,[3] Lorraine A. Remer,[1] and Yinon Rudich[4]

Received 8 April 2005; revised 10 June 2005; accepted 6 July 2005; published 30 July 2005.

REPORTS

Measurement of the Effect of Amazon Smoke on Inhibition of Cloud Formation

Ilan Koren,[1,2]* Yoram J. Kaufman,[1] Lorraine A. Remer,[1] Jose V. Martins[1,3]

Urban air pollution and smoke from fires have been modeled to reduce cloud formation by absorbing sunlight, thereby cooling the surface and heating the atmosphere. Satellite data over the Amazon region during the biomass burning season showed that scattered cumulus cloud cover was reduced from 38% in clean conditions to 0% for heavy smoke (optical depth of 1.3). This response to the smoke radiative effect reverses the regional smoke instantaneous forcing of climate from –28 watts per square meter in cloud-free conditions to +8 watts per square meter once the reduction of cloud cover is accounted for.

methods used to determine cloud-top pressure; aspects of t
lators. Differences in observed distributions of optical thick
differences can be traced to different approaches to partly
ISCCP treats as homogeneous. These cover roughly 15% of
tically thinnest clouds. Instrument simulators cannot reproduce these differences because there is no wa
to synthesize partly cloudy pixels. Nonetheless, MODIS and ISCCP observations are consistent for all b
the optically thinnest clouds, and models can be robustly evaluated using instrument simulators by i
tegrating over the robust subset of observations.

32, L14828, doi:10.1029/2005

Relationship between aerosol and cloud fraction over Australia

Jennifer D. Small,[1] Jonathan H. Jiang,[1] Hui Su,[1] and Chengxing Zhai[1]

Received 30 August 2011; revised 20 October 2011; accepted 26 October 2011; published 2 December 2011.

[1] We study the relationships between aerosols, clouds, and large scale dynamics over a north coastal Australia (NCA) region and a southeast Australia (SEA) region during the period 2002–2009 to evaluate the applicability of the aerosol microphysics-radiation-effect (MRE) theory proposed by Koren et al. (2008) in a low aerosol environment. We use aerosol optical depth (τ_a), fire counts, and cloud fraction (f_c) from Aqua-MODIS, and NCEP Reanalysis vertical velocities at 500 mb (ω_{500}) as a proxy for dynamic regime. In the NCA we find a monotonic increase f_c (35%, absolute f_c) as a function of increasing τ_a. In the SEA, we find that f_c initially increases by 25% with increasing τ_a, followed by a slow systematic decrease (~18%) with higher τ_a. We show that the MRE theory proposed by Koren et al. (2008) adequately represents the variation of f_c with τ_a in both the NCA and SEA. By conditionally sorting data by ω_{500} we investigate the role dynamics plays in controlling the τ_a-f_c relationship and the rate at which f_c changes with τ_a. We find that the MRE theory can be used to empirically fit both $-\omega_{500}$ and $+\omega_{500}$ observations. By analyzing meteorological parameters from the NCEP Reanalysis, we find that variations in local meteorology are not likely the cause of the observed relationships of τ_a and f_c during biomass burning seasons. However, additional factors such as aerosol type and cloud type may play a role. **Citation:** Small, J. D., J. H. Jiang, H. Su, and C. Zhai (2011), Relationship between aerosol and cloud fraction over Australia, *Geophys. Res. Lett.*, *38*, L23802, doi:10.1029/2011GL049404.

increased aerosol results in higher cloud drop concentration, increased liquid water paths, cloud fraction, and higher albedo and thus longer cloud lifetime, has come under scrutiny in recent years. Local meteorology and dynamics are theorized to play several roles in modifying aerosol effects on clouds and precipitation via various pathways, including available precipitable water, relative humidity, and updraft velocities [*Loeb and Schuster*, 2008; *Dey et al.*, 2011]. *Yuan et al.* [2008] found that available water vapor explained 70% of the variance in the slope of the correlation found between drop effective radii and aerosol optical depth in their coastal study regions, while *Feingold et al.* [2001] found it had limited effect on their study of biomass burning aerosols in Brazil. *Ten Hoeve et al.* [2011] found that background column water vapor likely exerts a strong effect on cloud properties. High relative humidity (RH) at cloud base has been associated with positive correlations between cloud fractions and aerosol optical depth [*Loeb and Schuster*, 2008]. Changes in the local dynamics can also modify cloud microphysics and how the cloud system responds to aerosols. To prevent contamination by meteorological factors previous studies employ various techniques intended to cancel out or limit their effects such as spatial and temporal averaging or specific sorting and filtering criteria [*Kaufman and Nakajima*, 1993; *Loeb and Schuster*, 2008; *Huang et al.*, 2009; *Grandey and Stier*, 2010]. Recently, *Koren et al.* [2008] put forth a theory that predicts both an increase and decrease in f_c with τ_a. We refer to this theory here as the combined microphysical–radiative effect, or MRE. For

Other MODIS Atmosphere Products

- **Water Vapor**
  - During the daytime, a near-infrared algorithm is applied over clear land areas of the globe and above clouds over both land and ocean. Over clear ocean areas, water-vapor estimates are provided over the extended glint area.
- **Atmospheric Profile**
  - Total-ozone burden, atmospheric stability, temperature and moisture profiles, and atmospheric water vapor. All of these parameters are produced day and night for Level 2 at 5x5 1-km pixel resolution when at least 9 FOVs are cloud free.
- **Cloud Mask**
  - Indicates whether a given instrument field of view (FOV) of the Earth's surface is unobstructed by clouds or affected by cloud shadows.
- **Joint Atmosphere**
  - The post-launch Joint Atmosphere Product contains a spectrum of key parameters gleaned from the complete set of standard at-launch Level 2 products stored at 5-km and 10-km

MODIS Land Products

- **https://modis-land.gsfc.nasa.gov/#**
- **Land Products**
  - Surface Reflectance – Atmospheric Correction
  - Surface Reflectance BRDF/Albedo Parameter
  - Burned Area
  - Thermal Anomalies/Fire
  - Leaf Area Index – FPAR
  - Vegetation Cover Conversion, Continuous Fields
  - Snow and Sea Ice cover

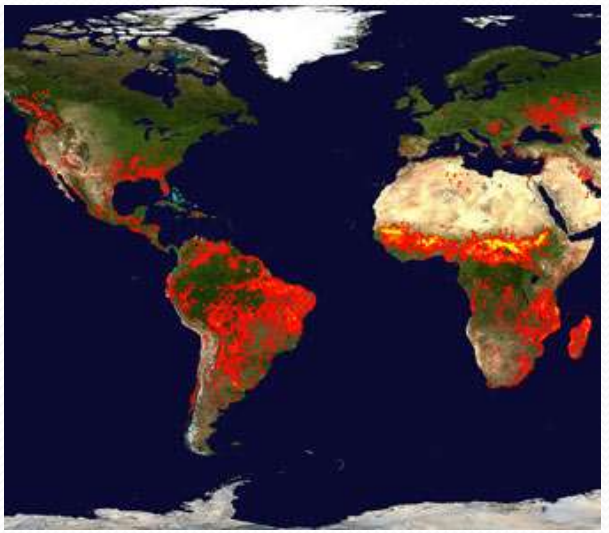

Product Name	Combined Terra & Aqua Product ID
Burned Area Monthly L3 Global 500m (MCD64)	MCD64A1
Burned Area Monthly L3 Global 500m (MCD45)	MCD45A1

Product Name	Terra Product ID	Aqua Product ID
Thermal Anomalies/Fire Daily L3 Global 1km	MOD14A1	MYD14A1
Thermal Anomalies/Fire 8-Day L3 Global 1km	MOD14A2	MYD14A2
Thermal Anomalies/Fire 5-Min L2 Swath 1km	MOD14	MYD14

MODIS Land Research Examples

Global products of vegetation leaf area and fraction absorbed PAR from year one of MODIS data

R.B. Myneni [a,*], S. Hoffman [a], Y. K
Y. Wang [a], X. Song [a], Y. Zhang [a], G.R
P. Votava [c], R.I

[a]Department of Geography, Boston Uni
[b]Biospheric Sciences Branch, NASA
[c]School of Forestry,

Relationship between MODIS fire hot spot count and burned area in a degraded tropical peat swamp forest in Central Kalimantan, Indonesia

K. Tansey [1], J. Beston [1], A. Hoscilo [1], S. E. Page [1], and C. U. Paredes Hernández [1]

Global estimation of burned area using MODIS active fire observations

L. Giglio[1], G. R. van der Werf[2], J. T. Randerson[3], G. J. Collatz[4], and P. Kasibhatla[5]

[1]Science Systems and Applications, Inc., NASA Goddard Space Flight Center, Greenbelt, Maryland, USA
[2]Department of Hydrology and Geo-Environmental Sciences, Vrije Universiteit, Amsterdam, The Netherlands
[3]Department of Earth System Science, University of California, Irvine, California, USA
[4]NASA Goddard Space Flight Center, Greenbelt, Maryland, USA
[5]Nicholas School of the Environment and Earth Sciences, Duke University, Durham, North Carolina, USA

Received: 2 September 2005 – Published in Atmos. Chem. Phys. Discuss.: 1 November 2005
Revised: 13 January 2006 – Accepted: 6 February 2006 – Published: 28 March 2006

Abstract. We present a method for estimating monthly burned area globally at 1° spatial resolution using Terra MODIS data and ancillary vegetation cover information. Using regression trees constructed for 14 different global regions, MODIS active fire observations were calibrated to burned area estimates derived from 500-m MODIS imagery based on the assumption that burned area is proportional

annual burned area for the years 2001–2004 to vary between 2.97 million and 3.74 million km^2, with the maximum occurring in 2001. These coarse-resolution burned area estimates may serve as a useful interim product until long-term burned area data sets from multiple sensors and retrieval approaches become available.

ber 2008.

ermal wavelengths.
n shown to be
rmally with a flaming
igh-quality burned
ned area when
iomass burning. We
spatially variable and
icle, we explore the
legraded and partially
sia. MODIS thermal
g constellation (DMC)
alculate a figure
levels of hotspot
fidence levels best
elatively small number
all number of
for each hotspot were
rder of 60%; hotspot

MODIS Ocean Products

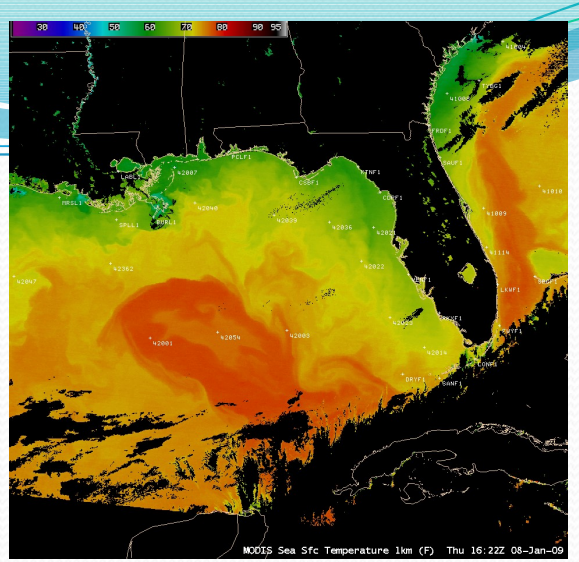

- https://oceancolor.gsfc.nasa.gov/about/
- **Ocean Products – (for both Terra and Aqua)**
  - Ocean Color
  - Sea Surface Temperature
  - Chlorophyll Concentration (two algorithms)
  - Absorption due to gelbstoff, detrital material and phytoplankton
  - Calcite Concentration
  - Diffuse attenuation
  - Flourescence Line Height
  - Instantaneous Photosynthetically Available Radiation
  - Particulate Organic Carbon
  - Particulate backscattering
  - Reflectance (at a bunch of wavelengths)
  - Total Absorption
  - Total Backscattering (at a bunch of wavelengths)

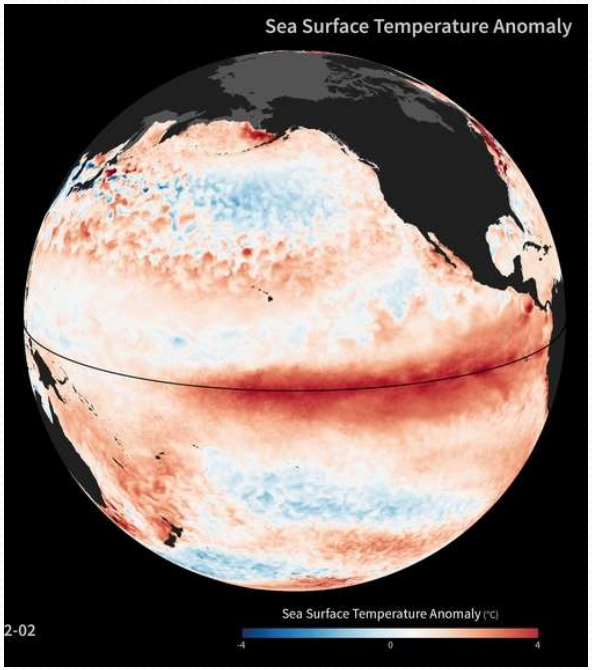

MODIS Ocean Research Examples

EOS

EOS, TRANSACTIONS, AMERICAN GEOPHYSICAL UNION

SST Data Improve Modeling of North American Monsoon Rainfall

PAGES 457, 462

The North American Monsoon System (NAM is the large-scale atmospheric circulation th results from complex ocean-atmosphere-lai interactions. It strongly modulates the summ weather/climate over Mexico and the south western United States. From June to Septemb NAMS precipitation provides much-needed water for the semi-arid region, and is also th

El Niño Southern Oscillation and vegetation dynamics as predictors of dengue fever cases in Costa Rica

D O Fuller[1,5], A Troyo[2] and J C Beier[3,4]

[1] Department of Geography and Regional Studies, University of Miami, Coral Gables,

Forecasting Fire Season Severity in South America Using Sea Surface Temperature Anomalies

Yang Chen,[1*] James T. Randerson,[1] Douglas C. Morton,[2] Ruth S. DeFries,[3] G. James Collatz,[2] Prasad S. Kasibhatla,[4] Louis Giglio,[5] Yufang Jin,[1] Miriam E. Marlier[6]

Fires in South America cause forest degradation and contribute to carbon emissions associated with land use change. We investigated the relationship between year-to-year changes in fire activity in South America and sea surface temperatures. We found that the Oceanic Niño Index was correlated with interannual fire activity in the eastern Amazon, whereas the Atlantic Multidecadal Oscillation index was more closely linked with fires in the southern and southwestern Amazon. Combining these two climate indices, we developed an empirical model to forecast regional fire season severity with lead times of 3 to 5 months. Our approach may contribute to the development of an early warning system for anticipating the vulnerability of Amazon forests to fires, thus enabling more effective management with benefits for climate and air quality.

Deforestation and forest degradation in South America contribute to anthropogenic carbon emissions and regional and global climate change (*1*–*4*). Fire is the dominant method for converting forest to cropland or pasture (*5*, *6*), and fires account for approximately half of the carbon emissions from deforestation and forest degradation in South America (*2*). Although deforestation rates in the Brazilian Amazon have declined over the past 5 years (*7*), trends in fires and burned area have not declined by the same amount, possibly because continued use of fire after deforestation maintains the risk of agricultural fires escaping into adjacent forests (*5*, *8*). Notably, extensive burning in the Brazilian states of Mato Grosso and Pará during 2007 led to the highest fire emissions of any year during the period 1997–2009 (*9*), highlighting the need to target forest degradation in addition to deforestation for sustained reductions in land use emissions from the region.

Projected decreases in Amazon rainfall during the 21st century (*10*, *11*) may increase the risk of forest fires (*12*), with the potential for larger carbon losses (*13*) and a positive feedback to climate change (*14*). Hence, the success of future climate mitigation and adaptation strategies will depend in part on more effective ways to manage fires. Advance information about the likelihood of fires in the dry season allows time to explore and implement management options such as allocation of firefighting resources or targeted burning restrictions.

[1]Department of Earth System Science, University of California, Irvine, CA 92697, USA. [2]NASA Goddard Space Flight Center, Biospheric Sciences Branch, Greenbelt, MD 20771, USA. [3]Department of Ecology, Evolution, and Environmental Biology, Columbia University, New York, NY 10027, USA. [4]Nicholas School of the Environment, Duke University, Durham, NC 27708, USA. [5]Department of Geography, University of Maryland, College Park, MD 20742, USA. [6]Department of Earth and Environmental Sciences, Columbia University, New York, NY 10027, USA.

*To whom correspondence should be addressed. E-mail: yang.chen@uci.edu

face
ion

CloudSat Cloud Profiling Radar

- http://cloudsat.atmos.colostate.edu/
- The Cloud Profiling Radar (CPR) is a 94-GHz nadir-looking radar which measures the power backscattered by clouds as a function of distance from the radar and produces detailed images of cloud structures.

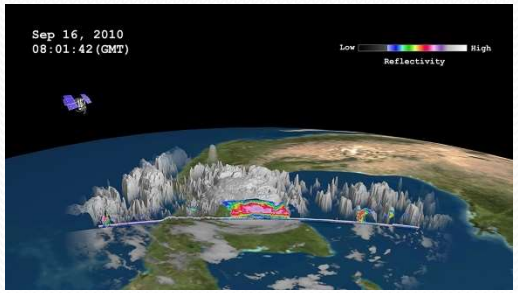

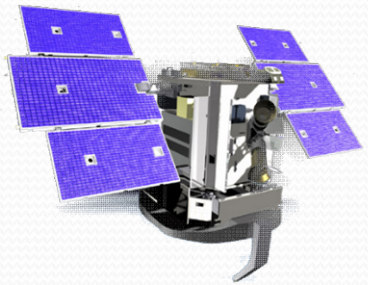

Product ID	Product Name	Responsible Persons
1B-CPR-FL	Radar Backscatter Profiles (First-Look)	Steve Durden
1B-CPR	Radar Backscatter Profiles	Steve Durden
2B-GEOPROF	Cloud Geometrical Profile	Jay Mace
2B-CLDCLASS	Cloud Classification	Zhien Wang
2B-CWC-RO	Cloud Water Content (Radar-only) (Includes liquid and Ice)	Norm Wood
2B-TAU	Cloud Optical Depth	John Haynes
2B-CWC-RVOD	Cloud Water Content (Radar-Visible Optical Depth) (Includes liquid and Ice)	Norm Wood
2B-FLXHR	Fluxes and Heating Rates	Tristan L'Ecuyer
2B-GEOPROF-LIDAR	Radar-Lidar Cloud Geometrical Profile	Jay Mace
2B-CLDCLASS-LIDAR	Radar-Lidar Cloud Classification	Zhien Wang
2B-FLXHR-LIDAR	Radar-Lidar Fluxes and Heating Rates	Tristan L'Ecuyer
2C-PRECIP-COLUMN	Column Integrated Precipitation Retrieval	John Haynes
2C-RAIN-PROFILE	Range Resolved Precipitation Retrieval	Matt Lebsock
2C-ICE	Ice Microphysical Retrieval	Jay Mace
2C-SNOW-PROFILE	Range Resolved Snowfall Retrieval	Norm Wood
2D-CLOUDSAT-TRMM	CloudSat/TRMM Matchups	Kwo-Sen Kuo
2D-CLOUDSAT-POES	CloudSat/NOAA 15-19 and MetOp-A Matchups	Kwo-Sen Kuo
2D-CLOUDSAT-TC	CloudSat/Tropical Cyclone Matchups	Natalie Tourville

CloudSat Cloud Profiling Radar

- **Temporal Coverage:**
  - June 2006 - Present
  - Swath data made up of Granules
  - Granules are 1 full orbit or 40, 022 km
- **Spatial Coverage:**
  - 125 vertical bins with approximately 240 m vertical spatial resolution
  - There are 31 Subsets for each granules
  - Each granule is made up of profiles

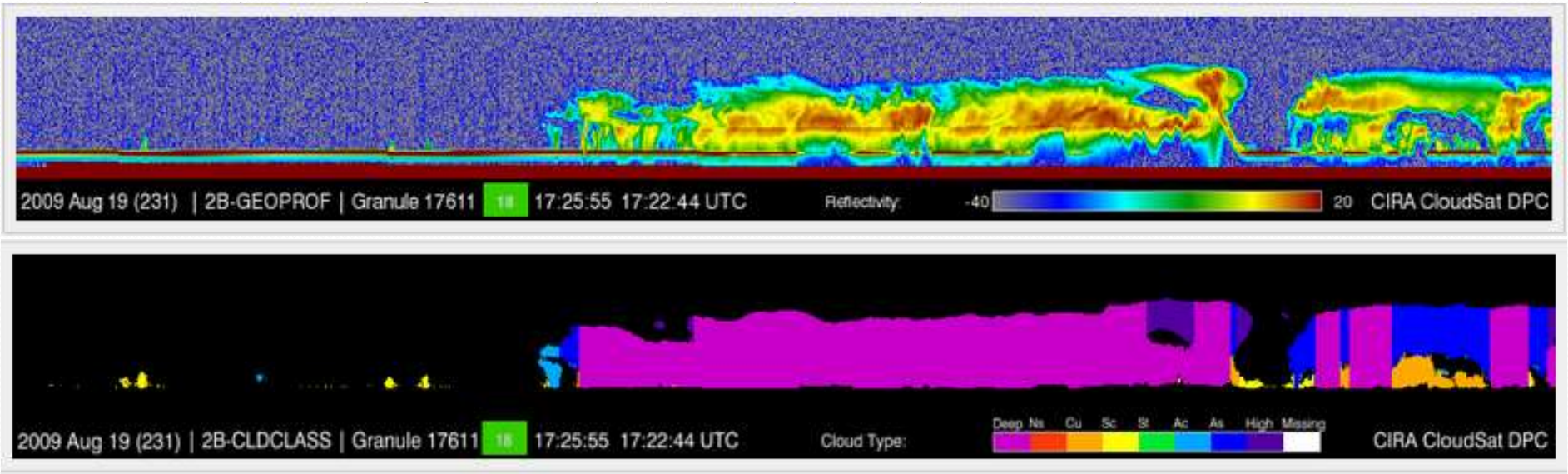

CloudSat Cloud Profiling Radar

- Quick Looks help you choose a Granule
- Good for specific events
- Climatologies, when looking at full data set averaged over long time periods.

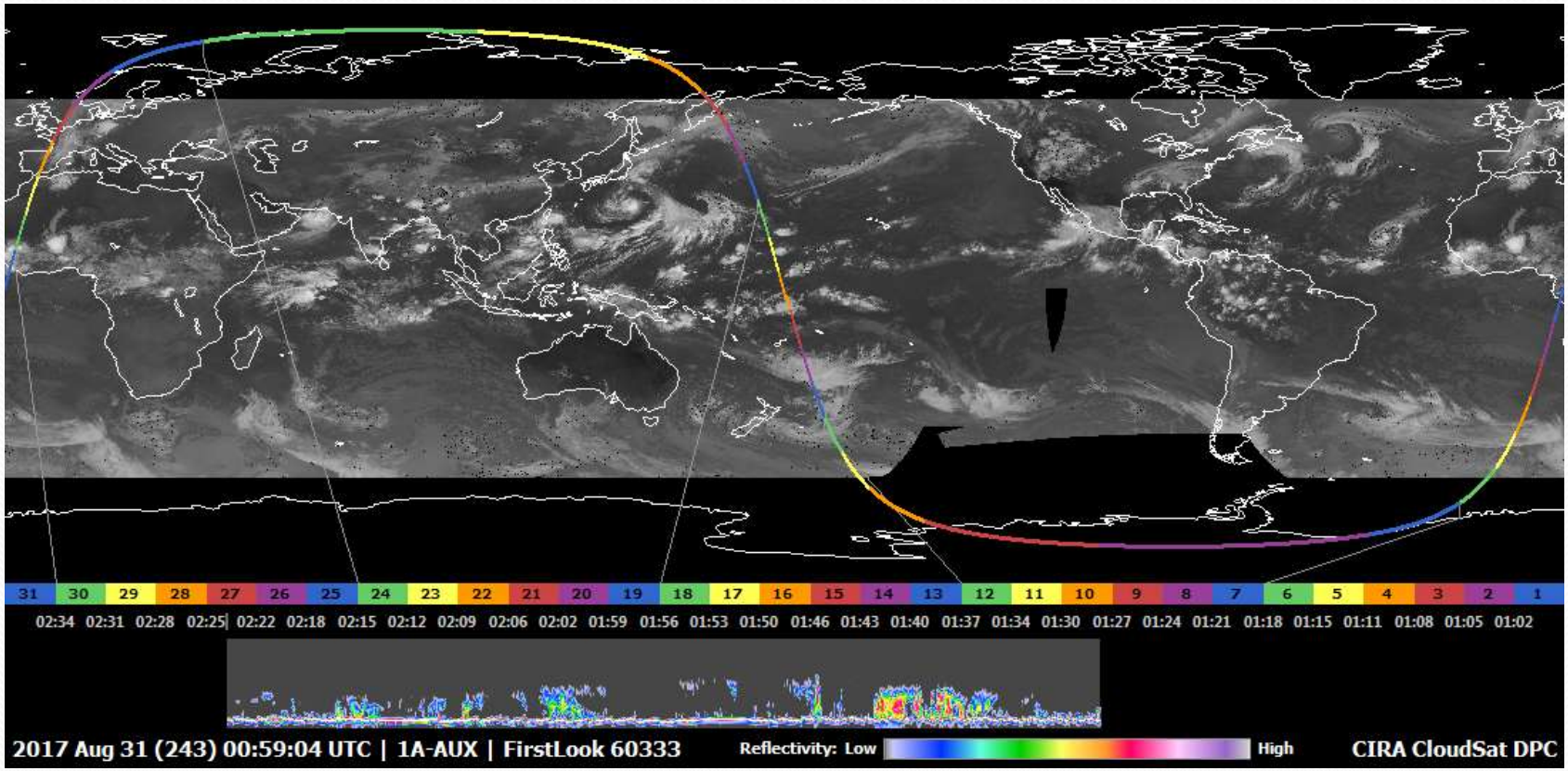

CloudSat Research Examples

CloudSat measurements of landfalling hurricanes Gustav and Ike (2008)

Sergey Y. Matrosov[1]

Received 17 May 2010; revised 17 August 2010; accepted 24 August 2010; p

Cirrus clouds and deep convection in the tropics: Insights from CALIPSO and CloudSat

Kenneth Sassen,[1] Zhien Wang,[2] and Dong Liu[2]

Received 20 February 2009; revised 5 June 2009; accepted 30

[1] Using a 2-year data set of combined lidar Cloud-Aerosol Lidar and Infrared Pathfinder S CloudSat satellites, the occurrence of tropical c The cloud identification algorithm takes advar deep precipitating clouds and of the lidar to s Examined are the frequency of occurrence an clouds, and their apparent interconnections. Tl in tropical cirrus mainly over land, with signi compared to day, but no clear diurnal pattern daylight signal noise effects do not appear to pattern, because high, thin tropopause transitic diurnal effect. Stratifying the global results by we find that most of the planet's subvisual (τ and are more frequent at night and over ocear their highest global frequencies over equatorial and are also more frequent at night but occur ~3.0) cirrus are spread globally and tend to oc is unknown which of the several proposed cir in the tropics, the close association of cirrus v cirrus are linked to deep convective activity, v clouds.

Cloud Vertical Distribution across Warm and Cold Fronts in *CloudSat*–CALIPSO Data and a General Circulation Model

CATHERINE M. NAUD

t Applied Mathematics, Columbia University, New York, New York

ANTHONY D. DEL GENIO

Institute for Space Studies, New York, New York

Tropical oceanic cloudiness and the incidence of precipitation: Early results from CloudSat

John M. Haynes[1] and Graeme L. Stephens[1]

Received 12 January 2007; revised 16 March 2007; accepted 5 April 2007; published 10 May 2007.

[1] Results of analysis of CloudSat radar data collected during the first three months of operation are described. It is shown that the global tropical oceans (30N–30S) predominantly favor clouds with tops in two layers centered at about 2 and 12 km. Precipitating clouds occur primarily in three modes, a shallow mode that is the most frequent type, as well as a middle and deep mode. Regional features are also discussed. The Indian and western Pacific Oceans exhibit more predominantly high clouds and deeper precipitation features than the eastern Pacific and Atlantic. The occurrence of a mid-level mode of cloudiness and precipitation is shown to vary regionally, being particularly significant in the western Pacific. For all regions examined, precipitating clouds are observed to be deeper than non-precipitating clouds. Over the global tropical oceans, 18% of the clouds detected by CloudSat produce precipitation.

Citation: Haynes, J. M., and G. L. Stephens (2007), Tropical oceanic cloudiness and the incidence of precipitation: Early results from CloudSat, *Geophys. Res. Lett.*, *34*, L09811, doi:10.1029/2007GL029335.

Aqua satellite and in formation with the French PARASOL satellite and the EOS Aura satellite. This creates the A-Train satellite constellation [*Stephens et al.*, 2002]. In this note we report early results from the analysis of the first three months (June–July–August, JJA) of the Level 2B Geometrical Profiling product of CloudSat (hereafter 2B-GEOPROF). A simple method to identify precipitation is also introduced and is applied to the 2B-GEOPROF data to provide novel, global-in-scale information about tropical cloudiness and its related precipitation.

2. The CloudSat 2B-GEOPROF Data

[4] The CloudSat data products [*Stephens et al.*, 2002] are available at the CloudSat data processing center (http://cloudsat.cira.colostate.edu). Two important products currently available are the 1B-CPR product which contains the calibrated raw power profiles measured by the CPR, and the 2B-GEOPROF product now briefly described [see also *Mace et al.*, 2007]. The 2B-GEOPROF product contains two main types of information. The first is the cloud mask

CALIPSO

- https://www.nasa.gov/mission_pages/calipso/main/index.html
- Cloud-Aerosol Lidar and Infrared Pathfinder Satellite Observation combines an active lidar instrument with passive infrared and visible imagers to probe the vertical structure and properties of thin clouds and aerosols over the globe.

Table 1. CALIPSO Level 2 Aerosol and Cloud Measurements

Data Product	Measurement Capabilities and Uncertainties	Data Product Resolution	
		Horizontal	Vertical
Aerosols			
Height, Thickness	For layers with $\beta > 2.5 \times 10^{-4}$ km^{-1} sr^{-1}	5 km	60 m
Optical depth, τ	40% *	5 km	N/A
Backscatter, $\beta_a(z)$	20 - 30%	40 km 40 km	Z < 20 km 120 m Z ≥ 20 km: 360 m
Extinction, σ_a	40% *	40 km 40 km	Z < 20 km 120 m Z ≥ 20 km: 360 m
Clouds			
Height	For layers with $\beta > 1 \times 10^{-3}$ km^{-1} sr^{-1}	1/3, 1, 5 km	30, 60 m
Thickness	For layers with $\tau < 5$	1/3, 1, 5 km	60 m
Optical depth, τ	within a factor of 2 for $\tau < 5$	5 km	N/A
Backscatter, $\beta_c(z)$	20 - 30%	5 km	60 m
Extinction, σ_c	within a factor of 2 for $\tau < 5$	5 km	60 m
Ice/water phase	Layer by layer	5 km	60 m
Ice cloud emissivity, ε	±0.03	1 km	N/A
Ice particle size	±50% for $\varepsilon > 0.2$	1 km	N/A

Note: * assumes 30% uncertainty in the aerosol extinction-to-backscatter lidar ratio, S_a.

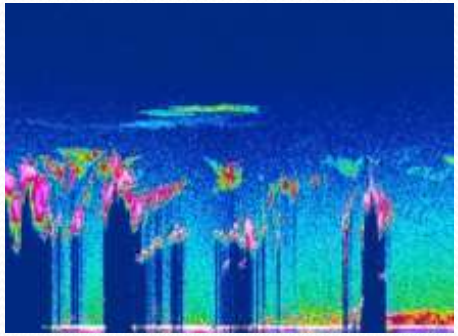

CALIPSO

- **Temporal Coverage:**
  - June 13, 2006 - Present
  - Swath data made up of Profiles and Layer Data
- **Spatial Coverage:**
  - Global (-90 x 90 and -180 x 180)
  - Spatial Resolution - 5 km

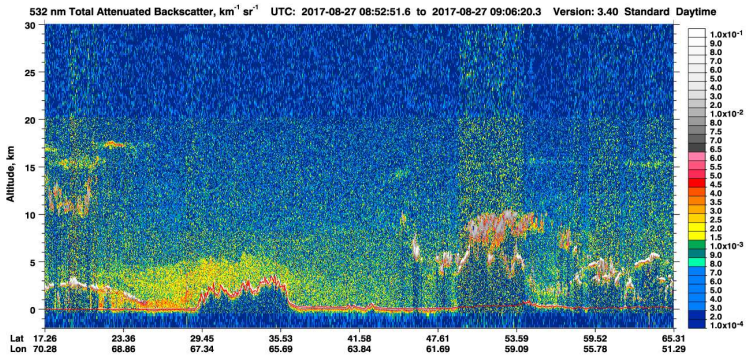

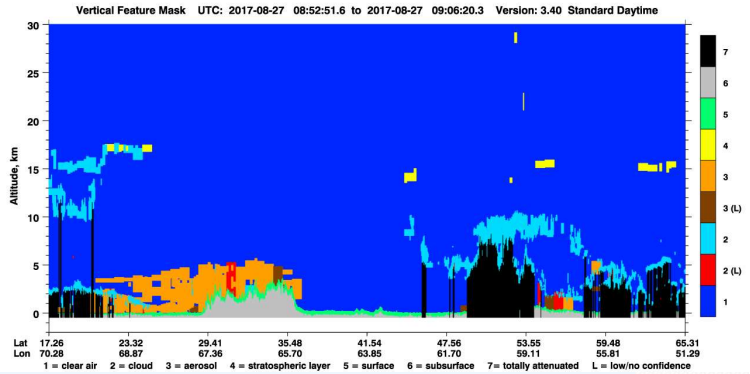

Home » Data Descriptions » Clouds » CALIPSO

CALIPSO IIR L1 V2-00 Release Announcement
CALIPSO Standard/Expedited Processing Suspended

CALIPSO Data and Information

Cloud-Aerosol Lidar and Infrared Pathfinder Satellite Observations (CALIPSO) was launched on April 28, 2006 to study the roles of clouds and aerosols of climate and weather. It flies in the international "A-Train" constellation for coincident Earth observations. The CALIPSO satellite comprises three instruments, the Cloud-Aerosol Lidar with Orthogonal Polarization (CALIOP Lidar), the Imaging Infrared Radiometer (IIR), and the Wide Field Camera (WFC). CALIPSO is a partnership between NASA and the French Space Agency, CNES.

Level 1B | Level 1.5 | Level 2 | Level 3 | Expedited Data | Read Software | Documentation

Instrument	Data Products
CALIOP Lidar	• Aerosol Profiles and Layers • Cloud Profiles and Layers • Merged Aerosol and Cloud Layers • Vertical Feature Mask • Polar Stratospheric Cloud
Imaging Infrared Radiometer (IIR)	• IIR along CALIOP Lidar Track • IIR Full Swath

CALIPSO

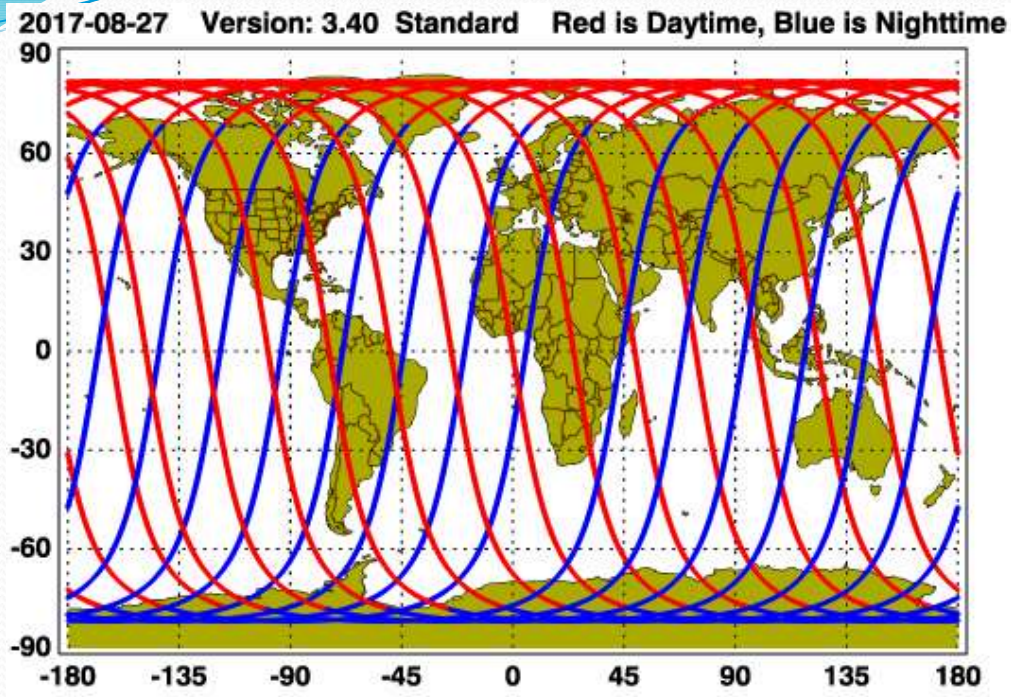

- There are a maximum of 4 scaled images per granule.
- The orbit tracks plotted on the maps show the measurement locations for each granule.
- For each granule, the scaled images are ordered from left to right and their locations along the orbit tracks are color coded as: image one, image two, image three, image four.

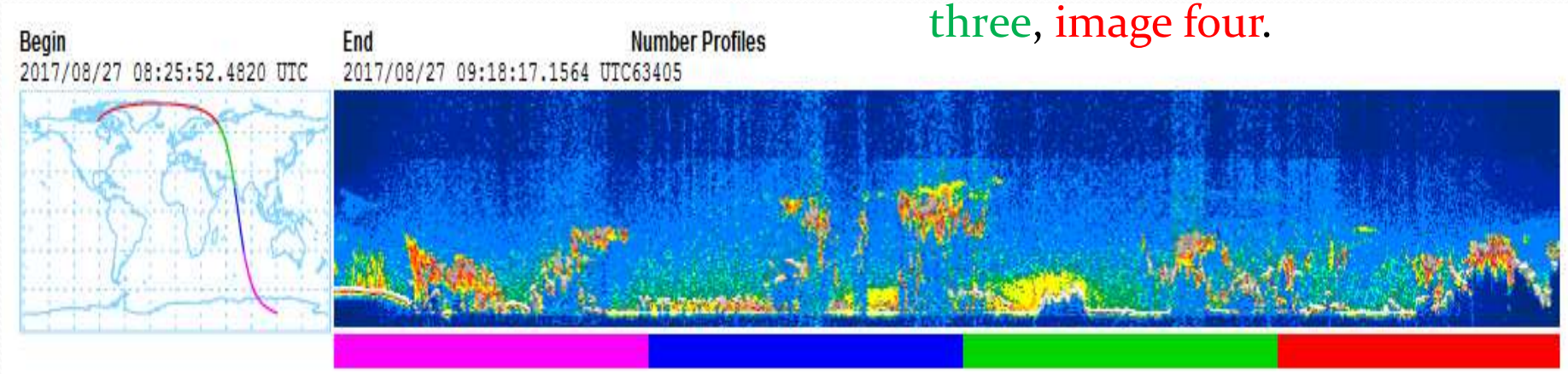

CALIPSO Research Examples

Patterns of North African dust transport over the Atlantic: winter vs. summer, based on CALIPSO first year data

Y. Ben-Ami, I. Koren, and O. Altaratz

Department of Environmental Sciences and Energy Research, Weizmann Institute of S

Received: 20 April 2009 – Published in Atmos. Chem. Phys. Discuss.: 15 June 2009
Revised: 11 September 2009 – Accepted: 22 September 2009 – Published: 20 October

CALIPSO lidar observations of the optical properties of Saharan dust: A case study of long-range transport

Zhaoyan Liu,[1] Ali Omar,[2] Mark Vaughan,[3] Johnathan Hair,[2] Chieko Kittaka,[3] Yongxiang Hu,[2] Kathleen Powell,[3] Charles Trepte,[2] David Winker,[2] Chris Hostetler,[2] Richard Ferrare,[2] and Robert Pierce[2]

lished 15 April 2008.

North Africa was observed
Satellite Observations
ved westward across the
f the event were examined
was acquired very near
over the Atlantic Ocean
1300 km and ~2400 km
ssed using measurements
RL over the Gulf of
sic optical properties of
sport over the Atlantic
hat have shown that there
e Atlantic. After the
in the lidar ratios, the
depolarization ratio
ations mentioned above,
phericity. The measured
.8 sr, respectively,
the Gulf of Mexico.
54 ± 13 and 44 ± 8.3 sr.
ments and with
064 nm are somewhat
g studies. The backscatter
0.01, and the optical
= 0.13, respectively.

Wildfire smoke injection heights: Two perspectives from space

Ralph A. Kahn,[1,2] Yang Chen,[1] David L. Nelson,[3] Fok-Yan Leung,[4] Qinbin Li,[1] David J. Diner,[1] and Jennifer A. Logan[4]

Received 27 September 2007; revised 5 December 2007; accepted 18 January 2008; published 22 February 2008.

[1] The elevation at which wildfire smoke is injected into the atmosphere has a strong influence on how the smoke is dispersed, and is a key input to aerosol transport models. Aerosol layer height is derived with great precision from space-borne lidar, but horizontal sampling is very poor on a global basis. Aerosol height derived from space-borne stereo imaging is limited to source plumes having discernable features. But coverage is vastly greater, and captures the cores of major fires, where buoyancy can be sufficient to lift smoke above the near-surface boundary layer. Initial assessment of smoke injection from the Alaska-Yukon region during summer 2004 finds at least about 10% of wildfire smoke plumes reached the free troposphere. Modeling of smoke environmental impacts can benefit from the combined strengths of the stereo and lidar observations.

Citation: Kahn, R. A., Y. Chen, D. L. Nelson, F.-Y. Leung, Q. Li, D. J. Diner, and J. A. Logan (2008), Wildfire smoke injection heights: Two perspectives from space, *Geophys. Res. Lett.*, *35*, L04809, doi:10.1029/2007GL032165.

[3] An independent investigation of smoke aerosol height, performed using data from the Cloud-Aerosol Lidar with Orthogonal Polarization (CALIOP) that flies aboard the joint US (NASA) and French (Centre National d'Etudes Spatiales/CNES) CALIPSO satellite, found that wildfire smoke remains in the boundary layer. It did not observe smoke aloft in a sampling of the CALIPSO global record, except in rare cases far from sources, after other atmospheric processes have had time to lift the smoke to higher elevations [*Labonne et al.*, 2007].

[4] The combination of MISR and CALIOP sampling and sensitivity differences may account for these seemingly disparate, qualitative conclusions about the frequency with which smoke is injected above the ABL. CALIOP is part of the A-Train constellation, having a dayside equator crossing at about 1:30 PM local time, and a field-of-view, before averaging, of 100 m [*Winker et al.*, 2004]. The MISR dayside equator crossing is at about 10:30 AM local time (about an hour later, local time, over most longitudes of Alaska), and its swath is nearly a factor of 4×10^3 wider

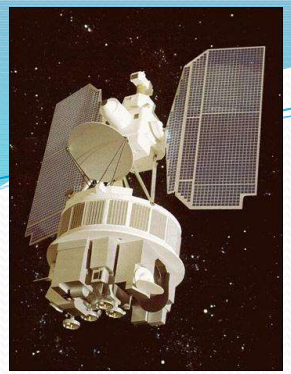

TOMS

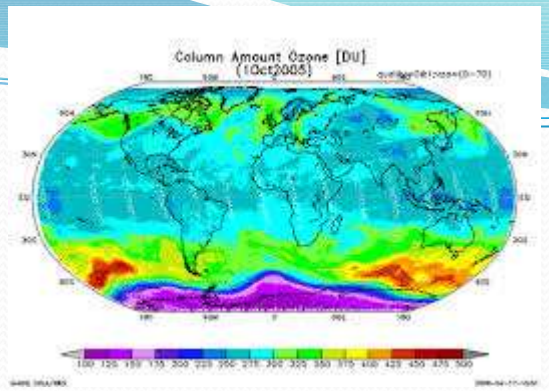

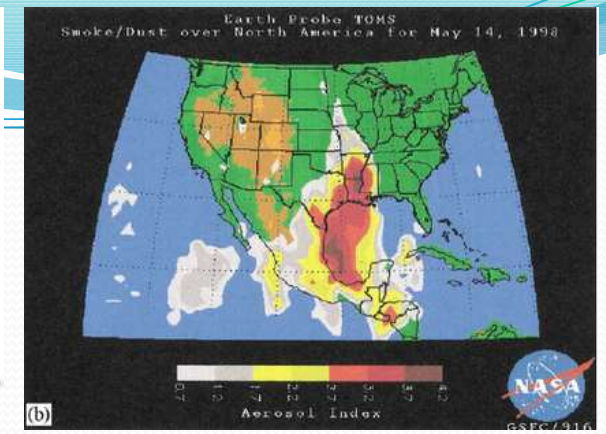

- https://eospso.gsfc.nasa.gov/missions/total-ozone-mapping-spectrometer-earth-probe

- **Total Ozone Mapping Spectrometer – Two different satellites**

- **Temporal Coverage:**
  - **DAILY Data**
  - Nimbus 7 (N7) – December 1978 to May 1993
  - Earth Probe (EP) – July 1996 to June 2006

- **Spatial Coverage (note products are at a lower resolution):**
  - N7 - The ground resolution is 47 km x 47 km at nadir and 62 x 62 km overall
  - EP - Nadir - 50 km x 50 km; average: 62 km x 62 km

TOMS

- Important data set for studying **Ozone and Ozone Holes** in the past.
- Useful for calculating **climatologies** of aerosol (specifically absorbing aerosol like smoke and dust).
- Useful for evaluating **historical events** involving aerosol such as volcanic eruptions, large dust storms and biomass burning.

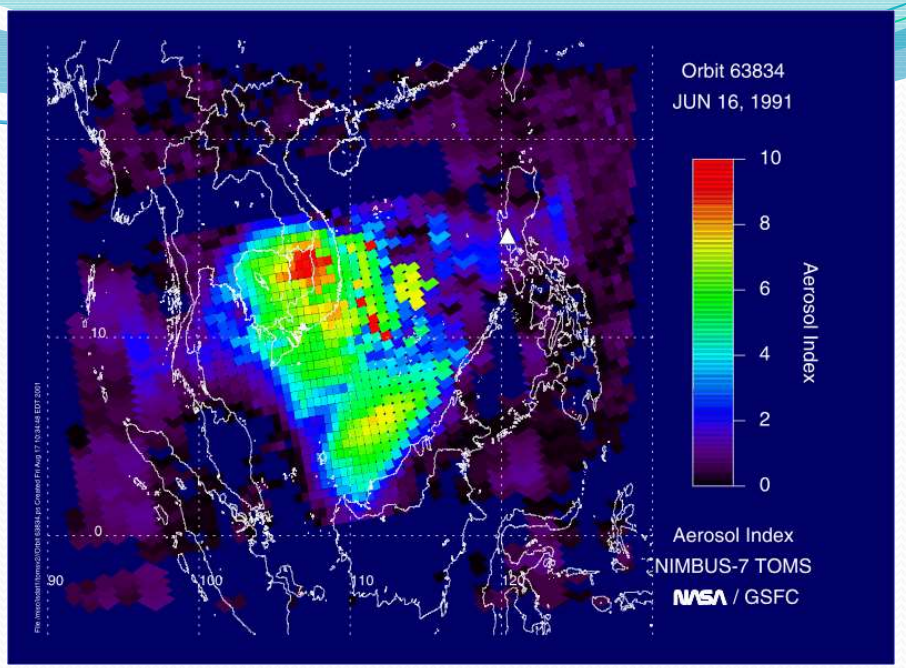

- Aerosol from Mt. Pinatubo in 1991

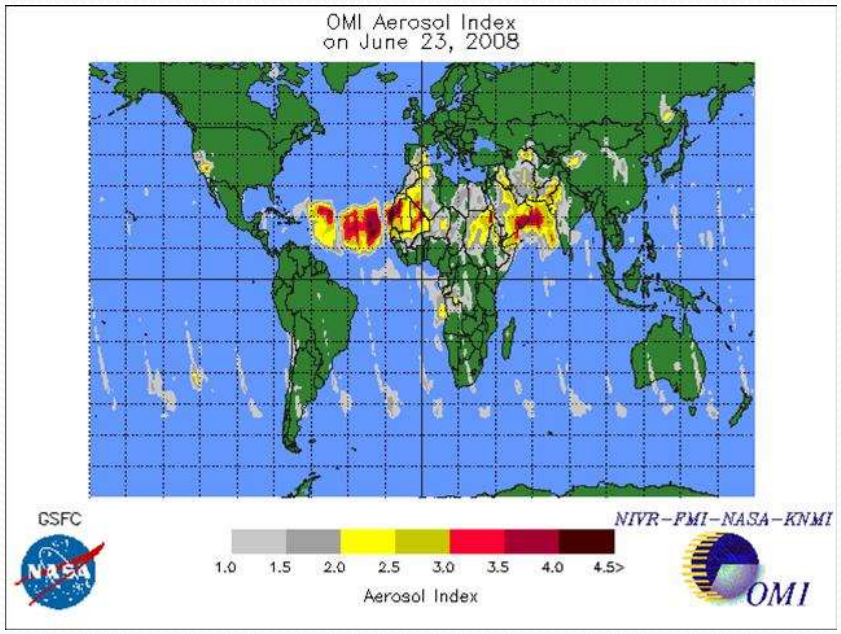

TOMS Research Examples

Satellite Detection of Smoke Aerosols Over A Snow/Ice Surface By TOMS

N. C. Hsu[1], J. R. Herman[2], J. F. Gleason[2], O

Abstract. A recently developed technique of using UV radiance measurements to aerosols is found to be effecti method takes advantage of the in the backscattered radiance d aerosols over snow/ice surfac distribution derived from Tota (TOMS) data is shown for a smoke generated by Canadian f Greenland. During this event reflectivity over the snow/ice s 90-100% down to 30-40%. smoke events over snow/ice interannual variability in th observed over Greenland.

Global distribution of UV-absorbing aerosols from Nimbus 7/TOMS data

J. R. Herman and P. K. Bhartia
Laboratory for Atmospheres, Goddard Space Flight Center, Greenbelt, Maryland

O. Torres, C. Hsu, and C. Seftor
Hughes STX Corporation, Greenbelt, Maryland

E. Celarier
Software Corporation of America, Lanham, Maryland

Abstract. Global distributions of UV-absorbing aerosols are obtained using measured differences between the 340 and the 380 nm radiances from the Nimbus 7 Total Ozone Mapping Spectrometer (TOMS) for the years 1979–1993. Time series are shown for major sources of biomass burning and desert dust giving the frequency of occurrence and areal coverage over land and oceans. Minor sources of UV-absorbing aerosols in the atmosphere are also discussed (volcanic ash and oil fires). Relative values of year-to-year variability of UV-absorbing aerosol amounts are shown for major aerosol source regions: (1) central South America (Brazil) near 10°S latitude; (2) Africa near 0°–20°S and 0° to 10°N latitude; (3) Saharan Desert and sub-Saharan region (Sahel), Arabian Peninsula, and the northern border region of India; (4) agricultural burning in Indonesia, Eastern China, and Indochina, and near the mouth of the Amazon River; and (5) coal burning and dust in northeastern China. The first three of these regions dominate the injection of UV-absorbing aerosols into the atmosphere each year and cover areas far outside of their source regions from advection of UV-absorbing particulates by atmospheric wind systems. During the peak months, smoke and dust from these sources are transported at altitudes above 1 km with an optical depth of at least 0.1 and can cover about 10% of the Earth's surface. Boundary layer absorbing aerosols are not readily seen by TOMS because the small amount of underlying Rayleigh scattering leads to a small signal. Significant portions of the observed dust originate from agricultural regions frequently within arid areas, such as in the Sahel region of Africa, especially from the dry lake-bed near Lake Chad (13.5°N, 14°E), and intermittently dry drainage areas and streams. In addition to drought cycle effects, this suggests there may be an anthropogenic component to the amount of dust injected into the atmosphere each year. Detection of absorbing aerosols and calculation of optical depths are affected by the presence of large-scale and subpixel clouds in the TOMS field of view.

Desert aerosol transport in the Mediterranean region as inferred from the TOMS aerosol index

E. Ganor
d and Beverly Sackler Faculty of Exact Sciences, Tel Aviv

12 April 2002; published 8 November 2002.

sert dust aerosols with local maxima of the
the long period. Being simpler than the
r method gives the same results. It was first
from the sources located at latitude ~16°N
)°N and longitude ~6°W exceed the sinks
tmosphere over North Africa is almost
of mineral desert dust in spring and in
source located around latitude 16°N and
maximum activity around April. The region
rs as a more variable source with maximum
cyclones, mobilize the already suspended
thward along the Mediterranean basin. A
opagation was applied to the study of dust
us to follow their dynamics. Identifiable
of the sea and then move eastward with a
ng, this motion continues at least up to the
r the dustplume is prevented from

EX TERMS: 0305 Atmospheric Composition and
mospheric Composition and Structure: Constituent
Chemical: Aerosols (0305); *KEYWORDS:* Aerosols,

OMI

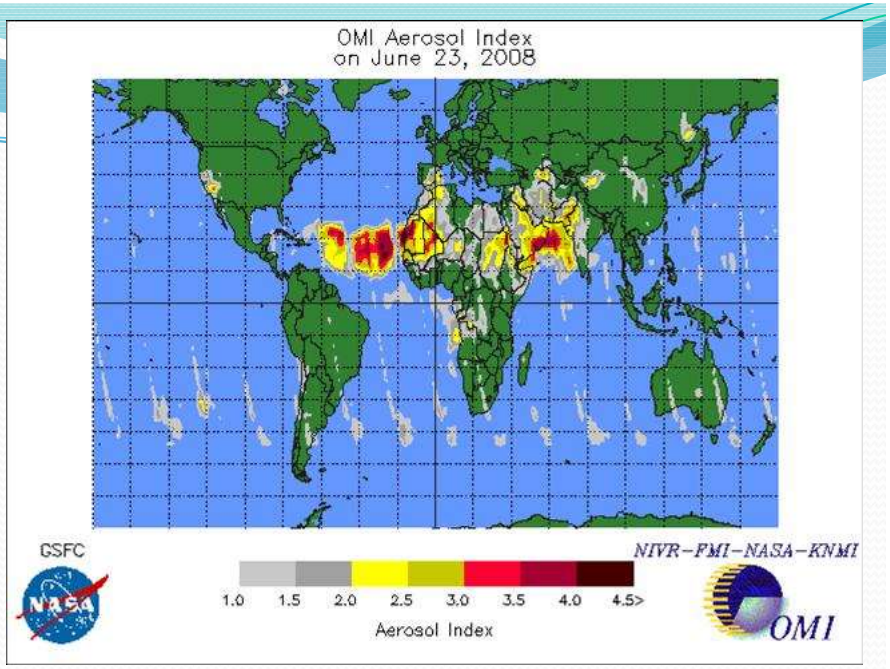

- https://aura.gsfc.nasa.gov/omi.html
- **Ozone Monitoring Instrument**
  - Distinguishes between aerosol types, such as smoke, dust, and sulfates, and measures cloud pressure and coverage, which provides data to derive tropospheric ozone.
  - OMI continues the TOMS record for total ozone and other atmospheric parameters related to ozone chemistry and climate. OMI measurements are highly synergistic with the other instruments on the Aura platform.
  - Measures atmospheric constituents including O_3, NO_2, SO_2, and aerosols such as dust, smoke and ash (especially absorbing aerosols), BrO, formaldehyde, and OClO (for chemistry in the stratosphere and troposphere).

OMI

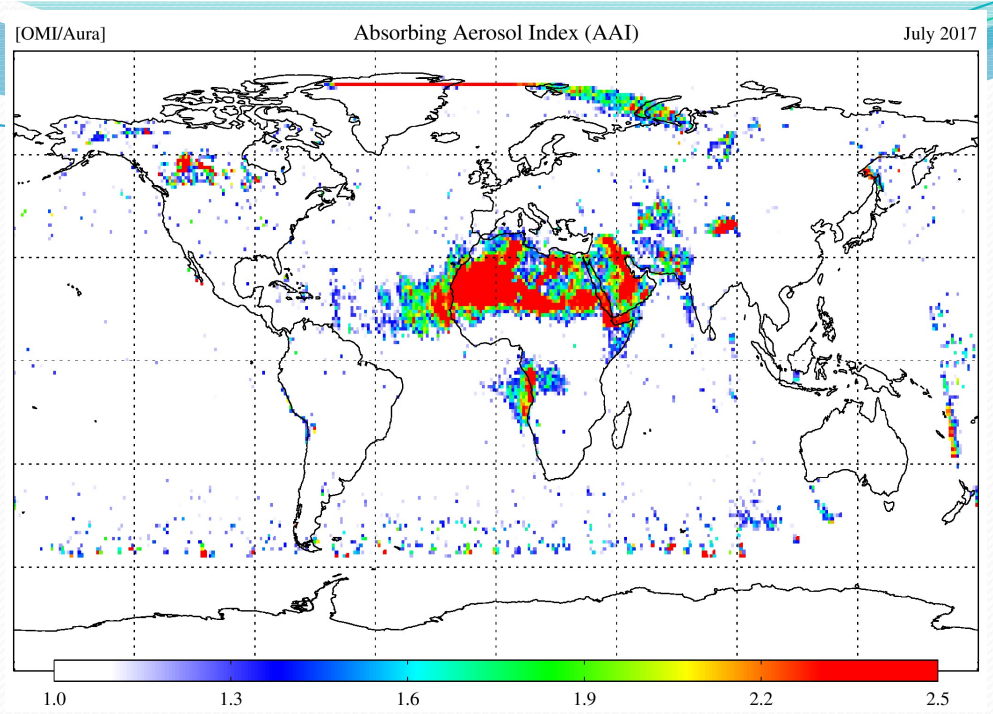

- **Temporal Coverage:**
  - **Swaths (fraction of day)**
  - **Daily Data**
  - October 2004 – Present
- **Spatial Coverage (note products are various resolutions):**
  - Varies based on format (Level 2 swath vs. Level 3 map)

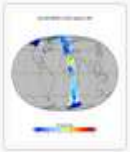 Hover	OMI/Aura Multi-wavelength Aerosol Optical Depth and Single Scattering Albedo 1-orbit L2 Swath 13x24 km V003 (OMAERO.003) - Aerosols	AURA OMI	1 hour	13 km x 24 km	2	2004-10-01	2017-08-31
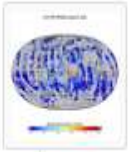 Hover	OMI/Aura Multi-wavelength Aerosol Optical Depth and Single Scattering Albedo L3 1 day Best Pixel in 0.25 degree x 0.25 degree V3 (OMAEROe.003) - Aerosols	AURA OMI	1 day	0.25 ° x 0.25 °	3	2004-10-01	2017-08-31

OMI Research Examples

An aerosol boomerang: Rapid around-the-world transport of smoke from the December 2006 Australian forest fires observed from space

Ruud J. Dirksen,[1] K. Folkert Boersma,[1] Jos de Laat,[1] Piet Stammes,[1]
Guido R. van der Werf,[2] Maria Val Martin,[3] and Hennie

Received 29 April 2009; revised 11 June 2009; accepted 21 July 2009; publi

[1] We investigate rapid around-the-world transport of a
intense forest fires in southeastern Australia in Decemb
December 2006, southeastern Australia suffered from s
high temperatures. On 14 December 2006, a passing co
the intense heat from the fires causing pyro-convective
aerosol particles into the jet stream. We track the resulti
Absorbing Index (AAI) observations from the Ozone M

Sulphur dioxide as a volcanic ash proxy during the April–May 2010 eruption of Eyjafjallajökull Volcano, Iceland

H. E. Thomas[1] and A. J. Prata[2]

[1]Department of Geological Engineering and Sciences, Michigan Technological University, Houghton, MI, USA
[2]Nordic Institute for Air Research (NILU), Kjeller, Norway

Received: 18 February 2011 – Published in Atmos. Chem. Phys. Discuss.: 7 March 2011
Revised: 20 June 2011 – Accepted: 20 June 2011 – Published: 18 July 2011

ruption having a considerable impact upon aviation in
pe. The closure of the majority of European airspace
17–19 April alone led to an estimated loss of $1.7 bil-
o the aviation industry (IATA, 2010). One of the most
ficant consequences of the eruption was the change in
safety policy from zero tolerance to the introduction of
oncentration thresholds (CAA, 2010). The International
Aviation Organization (ICAO) have now defined areas
w ($<2\times10^{-3}$ g m^{-3}), medium ($2–4\times10^{-3}$ g m^{-3}) and
($>4\times10^{-3}$ g m^{-3}) ash concentration to determine
e flight is allowable (low), allowable under certain
fic conditions (medium) or prohibited (high) (ICAO,
).
least 94 confirmed incidents were reported from 1953–
(Guffanti et al., 2010), where the most serious have
narrowly avoided catastrophe due to engine flame outs.
the current rapid rate of air traffic growth (ESCAP,
) there is the potential for many more such incidents and
the responsibility of the Volcanic Ash Advisory Cen-
VAACs) to provide advisories to the aviation industry
gh the effective modelling and monitoring of eruption
ls. Throughout the Eyjafjallajökull eruption, the Lon-
don VAAC at the UK Met Office was responsible for produc-
ing model predictions for the location of the ash cloud. Fol-

OMI and MODIS observations of the anomalous 2008–2009 Southern Hemisphere biomass burning seasons

O. Torres[1], Z. Chen[1], H. Jethva[1], C. Ahn[2], S. R. Freitas[3], and P. K. Bhartia[4]

[1]Dept. of Atmospheric and Planetary Sciences, Hampton University, Hampton, Virginia, USA
[2]Science Systems and Applications Inc., Lanham, Maryland, USA
[3]Center for Weather Forecasting and Climate Studies, INPE, Cachoeira Paulista, Brazil
[4]NASA Goddard Space Flight Center, Greenbelt, Maryland, USA

Received: 4 June 2009 – Published in Atmos. Chem. Phys. Discuss.: 13 October 2009
Revised: 17 March 2010 – Accepted: 18 March 2010 – Published: 16 April 2010

Abstract. Significant inter-annual variability of biomass burning was observed in South America over the 2007–2009 period. The 2007 number of fires detected from space in South America, as well as the magnitude of the atmospheric aerosol load resulting from fire activity, was the largest over the last ten years. The huge 2007 increase in fire activity was followed by large reductions in the 2008 and 2009 burning seasons. Large drops of the atmospheric load of aer-

most intense biomass burning season in the last ten years, the 2008 fire season was surprisingly weak. The combined analysis of satellite data on atmospheric aerosol load, fire counts and precipitation strongly suggests that the observed 2008 decline in aerosol load and fire activity in South America was heavily influenced by conditions other than meteorological factors.

monitoring both species concurrently.

TRMM

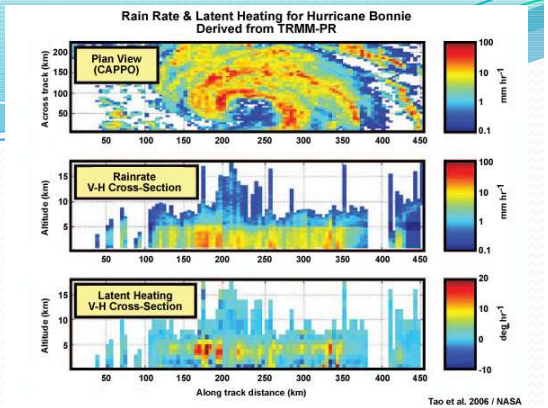

- https://pmm.nasa.gov/precipitation-measurement-missions

- **The Tropical Rainfall Measuring Mission (TRMM)**
  - Turned off on April 8. The spacecraft re-entered the Earth's atmosphere on June 15, 2015, at 11:55 p.m. EDT, over the South Indian Ocean
- Good for investigating historical events (from 1997-2015)
- Had 5 instruments
  - Precipitation Radar (PR)
  - TRMM Microwave Imager (TMI)
  - Visible Infrared Scanner (VIRS)
  - Lightning Images Sensor (LIS)
  - Cloud's and Earth's Radiant Energy System (CERES)

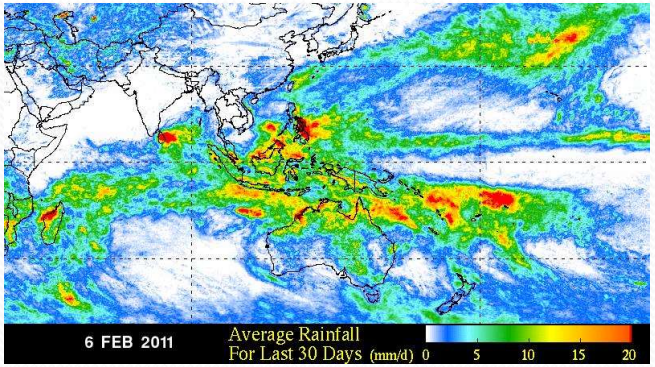

TRMM

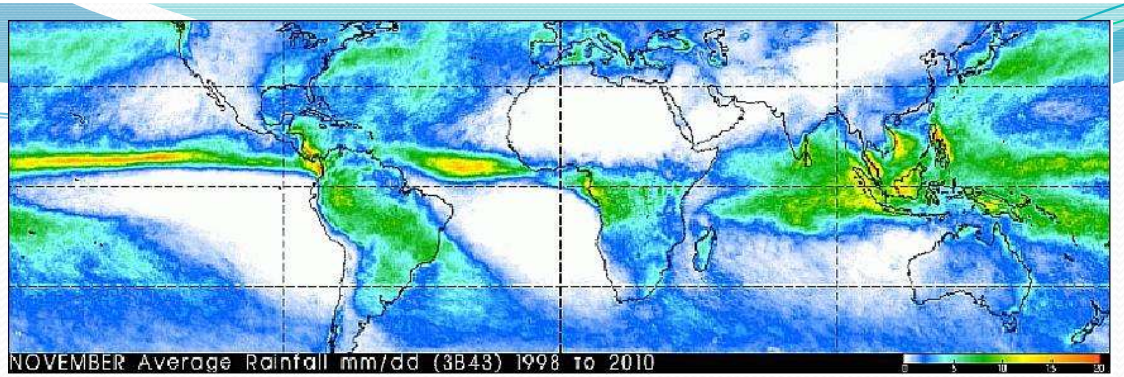

- **A Variety of Data Products are Available**
  - 3B42 Real Time Derived Daily Product and 10-Day Product
  - 3B42 Research Version and Derived Daily Product
  - 3B41 Real Time Rain rate estimated from geosynchronous infrared instruments
  - 3B40 Real Time Rain rate estimated from passive microwave radiometers
  - 3B43 Multi-satellite Precipitation
  - 3A46 SSM/1 Rain
  - 3B31 Combined Rainfall
  - 3A25 Surface Rain Total
  - 3A25 Spaceborne Radar Rainfall
  - 3A12 Mean 2A12, profile and surface Rainfall
  - 3A11 Oceanic Rainfall
- **Some products at 0.5 by 0.5 degrees (map)**
- **Some products – vertical structure**

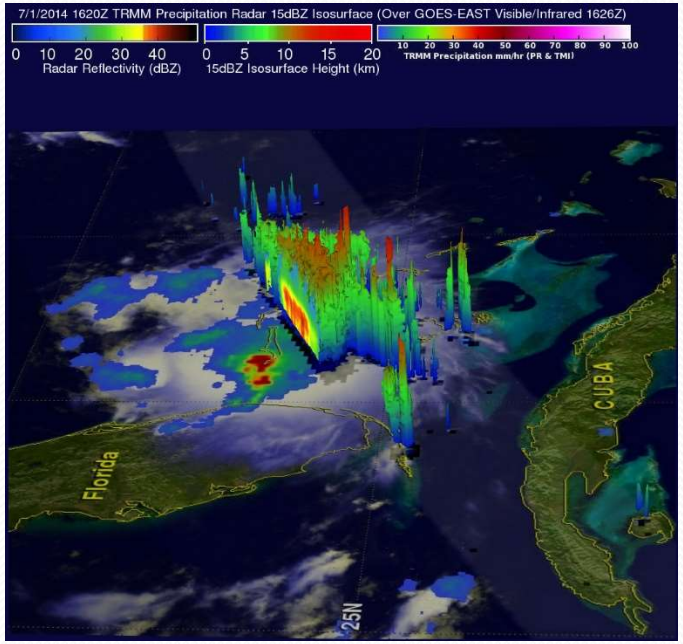

TRMM Research Examples

Tropical Rainfall Distributions Determined Using TRMM Combined with Other Satellite and Rain Gauge Information

ROBERT F. ADLER

Laboratory for Atmospheres, NASA Goddard Space Flight Center

GEORGE J. HUFFMAN AND DAVID T. BO

Laboratory for Atmospheres, NASA Goddard Space Flig
Science Systems and Applications, Inc., Greenbelt, M

Mechanisms for Diurnal Variability of Global Tropical Rainfall Observed from TRMM

SONG YANG

School of Computational Sciences, George Mason University, Fairfax, Virginia

ERIC A. SMITH

Maryland

January 2006)

ıbtropical rainfall are investigated
urements retrieved from the three
esults show that diurnal variability
providing assurance that TRMM
licipated, most ocean areas exhibit
ing daytime; however, important

um in late-evening–early-morning
mid- to late afternoon (MLA). In
he diurnal amplitudes. Amplitude
losely related to the rainfall accu-
distribution of diurnal variability
coexisting with the LE–EM maxi-
nvection. Analogously, there is a
tronger MLA maximum, although
ed with the large-scale circulation.
considered semidiurnal in nature.
convection is clearly an integral

f the diurnal cycle, indicating that
rscored by the appearance of sec-
g with other important features.
bility of seasonal rainfall over the
ıxima in spring and winter but only
bits double maxima in spring and
are also evident daytime maxima
t coasts of continents. The study
ıce either supports or repudiates
l rainfall variability.

Rainfall Climate Regimes: The Relationship of Regional TRMM Rainfall Biases to the Environment

WESLEY BERG, TRISTAN L'ECUYER, AND CHRISTIAN KUMMEROW

Department of Atmospheric Science, Colorado State University, Fort Collins, Colorado

(Manuscript received 3 January 2005, in final form 29 June 2005)

ABSTRACT

Intercomparisons of satellite rainfall products have historically focused on the issue of global mean biases. Regional and temporal variations in these biases, however, are equally important for many climate applications. This has led to a critical examination of rainfall estimates from the Tropical Rainfall Measuring Mission (TRMM) Microwave Imager (TMI) and precipitation radar (PR). Because of the time-dependent nature of these biases, it is not possible to apply corrections based on regionally defined characteristics. Instead, this paper seeks to relate PR–TMI differences to physical variables that can lead to a better understanding of the mechanisms responsible for the observed differences. To simplify the analysis, issues related to differences in rainfall detection and intensity are investigated separately. For clouds identified as raining by both sensors, differences in rainfall intensity are found to be highly correlated with column water vapor. Adjusting either TMI or PR rain rates based on this simple relationship, which is relatively invariant over both seasonal and interannual time scales, results in a 65%–75% reduction in the rms difference between seasonally averaged climate rainfall estimates. Differences in rainfall detection are most prominent along the midlatitude storm tracks, where widespread, isolated convection trailing frontal systems is often detected only by the higher-resolution PR. Conversely, over the East China Sea clouds below the ~18-dBZ PR rainfall detection threshold are frequently identified as raining by the TMI. Calculations based on in situ aerosol data collected south of Japan support a hypothesis that high concentrations of sulfate aerosols may contribute to abnormally high liquid water contents within nonprecipitating clouds in this region.

GPCP

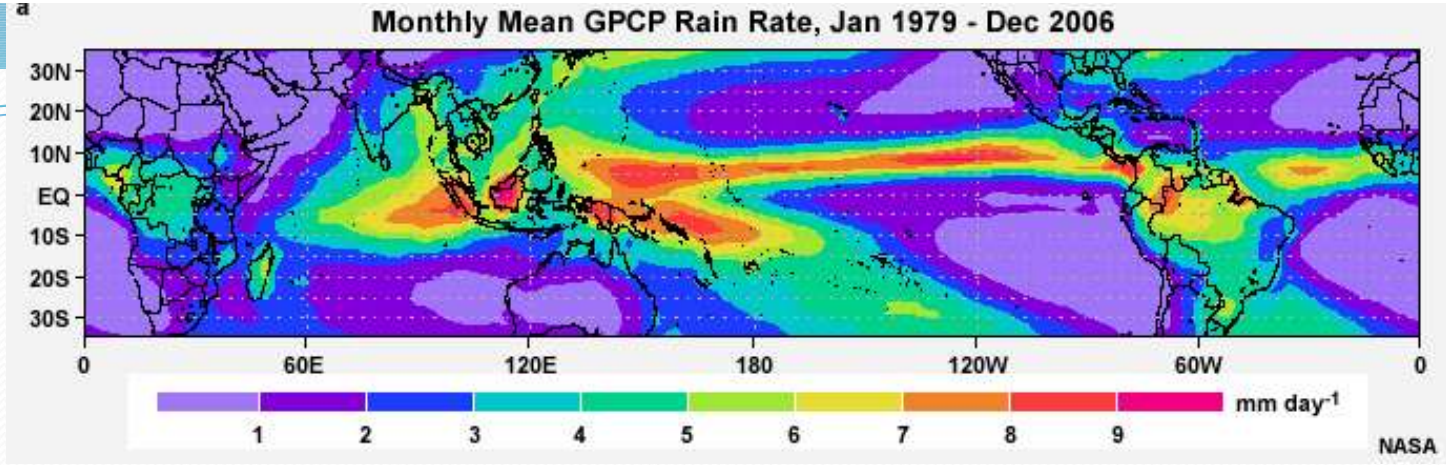

- https://precip.gsfc.nasa.gov/ **or** http://gpcp.umd.edu

- **Global Precipitation Climatology Project (V2.3)**
  - Global Precipitation Climatology Project monthly precipitation dataset from 1979-present combines observations and satellite precipitation data into 2.5°x2.5° global grids.

- **Temporal Coverage:**
  - Monthly values 1979/01 through Jun 2017 (some months are interim).
  - Long term monthly means, derived from years 1981 - 2010.

- **Spatial Coverage:**
  - 2.5 degree latitude x 2.5 degree longitude global grid (144x72)
  - 88.75N - 88.75S, 1.25E - 358.75E

GPCP

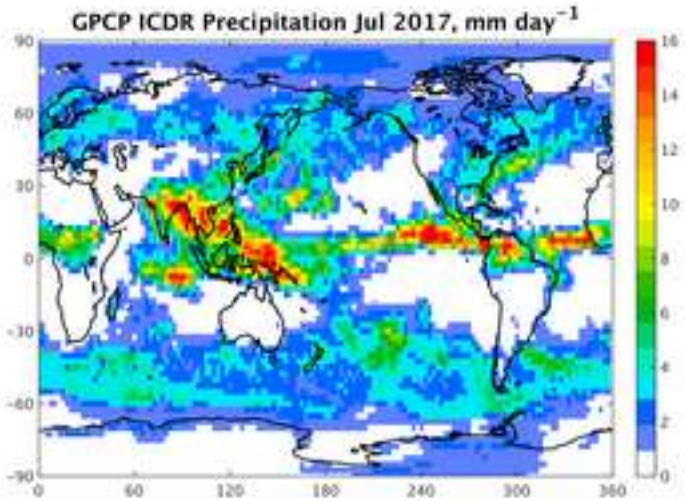

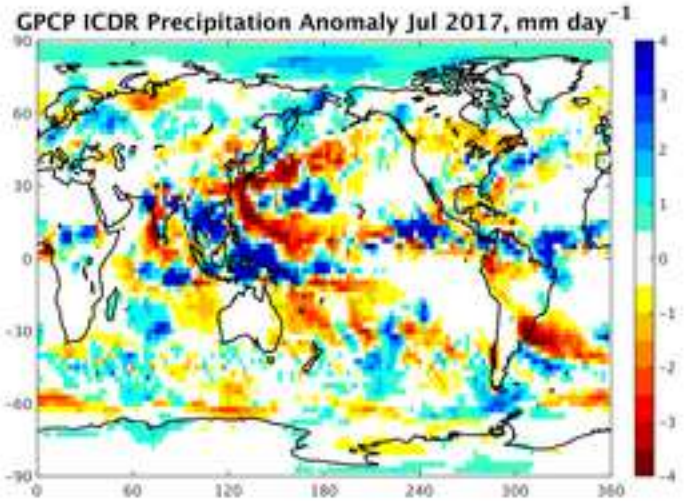

- The GPCP has been in existence for over twenty years as part of the Global Energy and Water Cycle Exchanges (GEWEX) effort under the World Climate Research Program (WCRP).
- The overall goal of GPCP is to provide the research and applications communities with high quality global analyses of precipitation at monthly and shorter time scales for climate analysis based on a combination of satellite and ground-based data sets.
- The GPCP data sets have been used in over 1500 articles in scientific journals and have become a standard in the analysis of global precipitation.

TRMM Research Examples

Changes in global monsoon precipitation over the past 56 years

Bin Wang[1] and Qinghua Ding[1]

Received 29 November 2005; revis

[1] Changes in the global m
examined using four sets o
sets compiled for the perio
diagnostic groups around t

INTERANNUAL VARIATIONS OF STORM TRACKS IN THE SOUTHERN HEMISPHERE AND THEIR CONNECTIONS WITH THE ANTARCTIC OSCILLATION

RGIO H. FRANCHITO
l de Pesquisas Espaciais,
razil

ied. Large interannual variations are
ominant periodicities. Some of these
torm track and the midlatitude spring
on (AAO) seems to be connected to
on between v_e and the AAO index in
orrelation in the subtropics are found
wind shear increases in the region of
of baroclinic eddies, i.e. increase of
lation in the midlatitudes between v_e
ndex phase the wind shear decreases
gative correlation between v_e and the

ENSO Modoki impact on the Southern Hemisphere storm track activity during extended austral winter

Karumuri Ashok,[1] C.-Y. Tam,[1,2] and W.-J. Lee[1]

Received 24 April 2009; accepted 2 June 2009; published 27 June 2009.

[1] Impacts of the recently discovered ENSO Modoki phenomena on extended winter storm track activity in the Southern Hemisphere are examined using the observed rainfall, sea surface temperature, and reanalyzed upper air circulation data for the period 1979–2004. The partial correlation technique is utilized to distinguish the impact of ENSO Modoki events from those of the ENSO and Indian Ocean Dipole (IOD). El Niño Modoki events introduce an anomalous blocking over central eastern Australia, which suppresses the storm track activity from southwest till centraleast, reducing the storm-associated rainfall in southeastern tip and portions of the southeast. On the other hand, the storm track activity in central Argentina is enhanced owing to the strengthened upper air westerlies in this region. The impacts from the ENSO Modoki events are apparently stronger than the individual impacts from the ENSO and IOD events. **Citation:** Ashok, K., C.-Y. Tam, and W.-J. Lee (2009), ENSO Modoki impact on the Southern Hemisphere storm track activity during extended austral winter, *Geophys. Res. Lett.*, *36*, L12705, doi:10.1029/2009GL038847.

eastern Indian Ocean and western Pacific in the southern hemisphere (see Figure 1a) [*Ashok et al.*, 2007a], with a subbranch along a subpolar jet further south. In the core region of the STJ over the western Pacific, the eddy amplitude decreases downstream, reaching its minimum over the central Pacific; the associated low-level storm track activity, however, is modest. In addition to the other issue that affects the storm track activity (see NS04), several studies propose that the ENSO events can influence the SH storm track activity by changing the strengths and positions of the STJ and/or the polar frontal jet (PFJ) in response to anomalous convective activity in the Tropics [*Trenberth et al.*, 1998; *Bhaskaran and Mullan*, 2003; *Nakamura et al.*, 2004; *Ashok et al.*, 2007a]. The anomalous convection associated with ENSO can influence the STJ via an anomalous divergent wind [*Sardeshmukh and Hoskins*, 1985], whereas the PFJ tends to be influenced through stationary Rossby waves generated in response to anomalous tropical convection [*Kidson et al.*, 2002]. *Ashok et al.* [2007a], generalizing the 1997 case study of *Nakamura et al.* [2004] to include all